Cellulose Nanofiber/Polyethylene Glycol Composite Phase Change Thermal Storage Gel Based on Solid-gel Phase Change

Yanghua CHEN *, Tingting WANG, Yanlei PEI

School of Advanced Manufacturing, Nanchang University, Nanchang 330031, No.999 Xuefu Road, Honggutan New District, Nanchang City, Jiangxi Province, China

http://doi.org/10.5755/j02.ms.35249

Received 3 October 2023; accepted 10 November 2023

In this paper, cellulose nanofiber (CNF)/ polyethylene glycol (PEG) composite aerogel phase change materials (CNPCMs) were prepared utilizing porous carrier support and freeze-drying. The solid-liquid phase change to solid-gel phase change was realized, which solved the problems of PEG flow, leakage, and shape instability. The physical properties and chemical compatibility of CNPCMs were studied, and the results showed that CNPCMs ensured the overall structure stability through internal hydrogen bonding, and they were only a physical bond with each other without chemical reaction. With the increase in PEG content, the thermal conductivity of CNPCMs increased from 0.22 W/m·K to 0.33 W/m·K. The thermal exposure experiment and thermogravimetric analysis (TGA) experiment have shown that CNPCMs have good shape stability at 75 ℃ and good thermal stability below 320 ℃. In summary, the experimental results indicated that the maximum content of PEG in CNPCMs was 78 % with an optimal content of 66.7 %. The sample corresponding to the optimal content was CNPCM2 with an enthalpy of 167.9 J/g for melting and 146.1 J/g for solidification. As a thermal storage material with good thermodynamic performance, CNPCM2 has enormous potential in the storage of solar collectors.

Keywords: composite aerogel phase change materials, hydrogen bond, heat storage, solid-gel phase change.

1. INTRODUCTION

More than a decade ago, we focused on extracting resources for economic development. The massive use of fossil fuels not only increases the consumption of resources but also causes serious pollution to the environment due to the large amount of smoke generated by combustion [1]. Therefore, the conflict between the environment and resources is becoming more and more intense. Environmental pollution caused by energy consumption is not immediately apparent, but has a lag [2], resulting in frequent natural disasters in recent years. We are aware of the harm caused by environmental pollution and have begun to reflect and vigorously study green, efficient, and sustainable methods and technologies. Thermal energy storage (TES) technology is one of them [3]. Its key role in improving energy utilization efficiency and solving the time-space imbalance of energy supply and demand is gradually being favored by researchers. TES includes sensible heat energy storage, latent heat energy storage, and thermochemical energy storage [4]. Compared with the other two methods, latent heat energy storage has a higher energy storage capacity and a more direct technical route [5, 6], so this paper focuses on the latent heat energy storage of phase change materials (PCMs).

Polyethylene glycol (PEG) is an ideal PCM for latent heat storage due to its stable property, controllable phase change temperature, and good dispersion [7]. However, it is prone to leakage after phase change [8, 9]. To address the leakage problem prevalent in PCMs, the researchers proposed three solutions [10]: solid-solid phase change, microencapsulation, and porous carrier support. Although solid-solid phase changes do not cause leakage problems, they are generally low in enthalpy [11]. For example, the phase change enthalpies of solid-solid phase change materials prepared by Xuemeng Fan's and Yan Zhou's team were 82.3 J/g and 118.7 J/g respectively [12, 13], which were still at a lower level than solid-liquid phase change materials. The shell material's encapsulation efficiency and mechanical strength must be considered by using the microencapsulation method [14]. In contrast, the porous carrier support method firmly confines the PCM in the porous carrier through hydrogen bonds, electrostatic interactions, and van der Waals forces or covalent bonds [10, 15], which can avoid the low enthalpy of the PCM and improve its mechanical strength at the same time.

CNF has the advantages of light weight, low density, high shape plasticity, and biodegradability [16]. It is widely used in energy storage [17], biopharming [18], wastewater treatment [19], 3D printing [20], and thermal insulation [21]. More importantly, it has great potential to improve the shape stability of PEG [22]. In this paper, based on the porous carrier support method and freeze-drying method [23], the solid-gel phase change of composite aerogel phase change materials (CNPCMs) was realized, which solved the problems of leakage and shape instability of PEG.

During the preparation of CNPCMs, the two steps of gelation and drying were particularly important, because different gelation and drying methods will affect the internal pore structure, morphology, and mechanical properties of nanocellulose-based porous material [24]. According to whether covalent bonds are involved, the gel mechanisms

* Corresponding author. Tel.: +86-13970944938
E-mail: *chenyh@ncu.edu.cn* (Y. Chen)

are divided into two categories [25]: (1) physical crosslinking, mainly by hydrogen bonds, electrostatic interactions, or van der Waals forces; (2) Chemical crosslinking. Compared with physical crosslinking, chemical crosslinking has better structural stability and mechanical strength [10, 26], but the preparation process is also more complex, and most of the experimental materials used are toxic. Both CNF and PEG have good dispersion, and simple physical crosslinking can meet the requirements of homogeneity and stability. The drying process is critical [27]. Yan Sun et al. [28] discussed three main drying methods for nanocellulose aerogels. They are supercritical drying, evaporative drying, and freeze drying. Supercritical drying is recognized as the most effective method to maintain pore microstructure [29], but its equipment is expensive, the process is complex, and the operation cost is high. Evaporative drying is a simple and economical method, but it is a challenge to avoid shrinkage and collapse of pore structures caused by capillary forces [28]. Therefore, we choose freeze-drying to avoid material collapse and make the pore structure more uniform [30]. The prepared CNPCMs can be used as heat storage material in the field of solar air collectors to improve efficiency.

2. EXPERIMENTAL SECTION

2.1. Materials

Polyethylene glycol 6000 (PEG) was purchased from Rohn Reagent Co. 1 wt.% mechanical grinding of cellulose nanofiber (CNF) hydrogel (length: 1 – 3 um, diameter: 5 – 20 nm, the surface functional group is the hydroxyl group, PH: 7 – 8) purchased from Huzhou ScienceK new material Technology Co., LTD. Ammonium persulfate (APS) was purchased from Sinopharm Holding Chemical Reagent Co., LTD., and N, N methylenebisacrylamide (MBA) was purchased from Aladdin Reagent Co., LTD. All materials were used as received materials and were not further purified.

2.2. Preparation of CNPCMs

Firstly, a certain amount of PEG powder was added to the beaker, heated in a water bath at 80 °C to melt it, and a certain proportion of CNF hydrogel was added. Next, after the two were mixed and heated in a water bath at 60 °C, and stirred for 1 min, MBA (as a physical crosslinker and thickener) and APS (as a polymerization initiator) were added. Then, the mixed solution was stirred for 3 hours and transferred to the oven at 60 °C for 3 hours to ensure complete polymerization. MBA and APS were added at 1 % of the overall mass of the solution, respectively. Finally, pour the mixed solution into the mold to complete the molding, put it in the freeze dryer for 12 hours (pre-freezing for 2 hours, vacuum drying for 10 hours), and remove it. According to the above method, by adjusting the ratio of CNF to PEG, samples of 1:1, 1:2, 1:4, 1:6, and 1:8 were designed, named as CNPCM1, CNPCM2, CNPCM3, CNPCM4, and CNPCM5, respectively. The preparation process of CNPCMs is shown in Fig. 1.

2.3. Characterization

A high-resolution field emission scanning electron microscope (FESEM, GeminiSEM 300, Britain) was used to observe the structural morphology. The chemical structures of CNF aerogel, PEG, and CNPCMs were analyzed by Fourier transform infrared spectroscopy (FTIR, Nicolet 5700, America) in the wave number range of 4000 ~ 400 cm^{-1} with a resolution of 4 cm^{-1}. The crystal structures of the samples were analyzed by an X-ray diffractometer (XRD, D8 ADVANCE, Germany). The phase change properties of the samples were characterized by differential scanning calorimetry (DSC, DSC 8000, America), and the samples were tested in the range of 0 to 100 °C with a heating and cooling rate of 10 °C/min under a nitrogen atmosphere. The thermal conductivity of the samples was determined by using the DRE-III multifunctional rapid thermal conductivity tester. The thermal stability of the samples was studied by using a thermogravimetric analyzer (TGA, TGA 4000, America) under nitrogen atmosphere at a temperature increase rate of 10 °C/min. PEG and CNPCMs were exposed to 60 °C and 75 °C in the oven to test the shape stability and leakage of the samples, and digital photographs were recorded in this experiment.

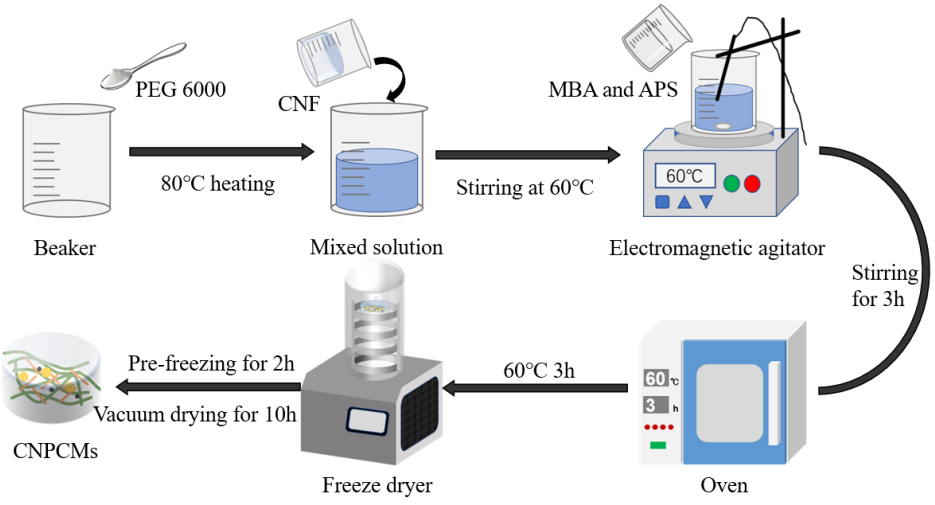

Fig. 1. Preparation process of CNPCMs

3. RESULTS AND DISCUSSION

3.1. Morphology

Both CNF (Fig. 2 a) and PEG have good dispersion, so uniformity can be achieved by simple melting mixing, and the prepared CNF/PEG was gel-like (Fig. 2 b). CNF can also be used as a natural thickener [31] which had a very excellent thickening effect. The physical crosslinking agent (MBA) added during the preparation process can quickly and efficiently transform the polymer from a linear structure to a three-dimensional network structure [32] and has a special thickening effect. The results showed that CNF/PEG gel had higher viscosity and stability, which laid a solid foundation for the solid-gel phase change mentioned in this paper. As shown in Fig. 2 c and Fig. 2 d, the CNF/PEG gel can remain non-flowing at the bottom when the beaker is inclined and inverted. CNF aerogel (Fig. 2 e) and CNPCMs (Fig. 2 g) obtained after freeze-drying for 12 hours did not shrink in volume, and there were pores on the surface. Fig. 2 f shows the morphology of PEG.

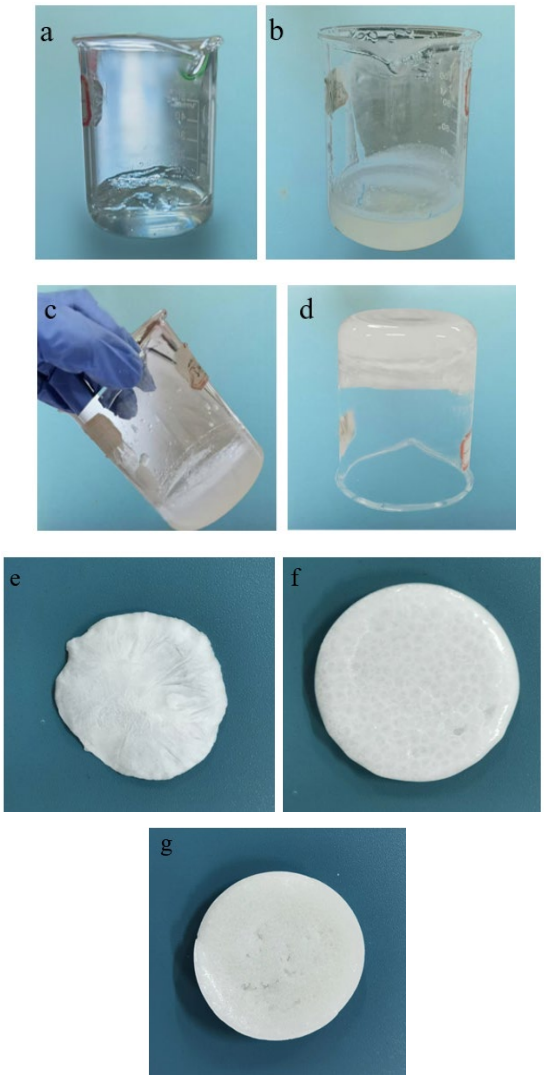

Fig. 2. Photos: a – CNF hydrogel; b – CNF/PEG hydrogel; c – an inclined vessel containing CNF/PEG hydrogel; d – an inverted vessel containing CNF/PEG hydrogel; e – CNF aerogel, f – PEG and g-CNPCMs

3.2. Microstructure analysis

The microstructures of CNF aerogel and CNPCMs were studied by scanning electron microscopy. The freeze-dried CNF aerogel had a connected porous structure (Fig. 3 a), which was conducive to high PEG loading. CNPCM1 (Fig. 3 b) and CNPCM2 (Fig. 3c) still had pore structures that firmly constrain PEG, thereby avoiding leakage. Because the PEG load of CNPCM2 was higher than that of CNPCM1, the internal structure of CNPCM2 was denser than that of CNPCM1 under SEM. With the increase in PEG load, the internal structure of CNPCMs became more and more compact. As can be seen from Fig. 3 d, Fig. 3 e, and Fig. 3 f, CNPCM3, CNPCM4, and CNPCM5 no longer had prominent pore structures. There was no clear boundary between CNF and PEG, and their close fit indicated that they had good compatibility.

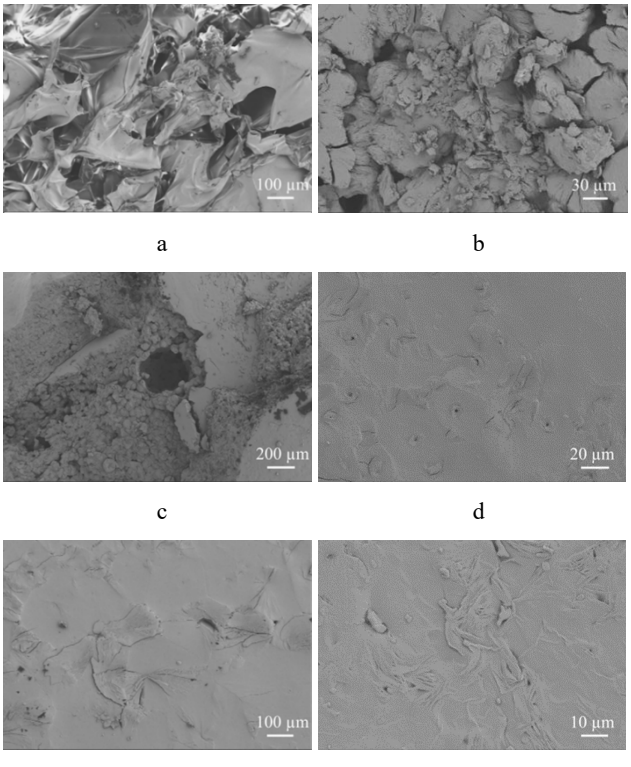

Fig. 3. SEM images: a – CNF aerogel; b – CNPCM1; c – CNPCM2; d – CNPCM3; e – CNPCM4; f – CNPCM5

3.3. FTIR analysis

As shown in Fig. 4, there were three sets of characteristic peaks in the spectrum of CNF aerogel near 3361 cm^{-1}, 2886 cm^{-1}, and 1108 cm^{-1}, namely O-H, C-H, and C-O stretching vibrations [17]. The spectra of PEG and CNPCMs showed the same peak around 2886 cm^{-1} and 1108 cm^{-1}. The peak observed at 1593 cm^{-1} corresponds to C=O stretching [33]. In CNPCMs, the absorption peak of C=C appeared at about 1651 cm^{-1} [9] and very mild O-H absorption peaks occurred near 3446 cm^{-1}. The shift of the O-H absorption peak indicated hydrogen bonds being formed [23]. The spectra of CNPCMs showed very small and sharp double peaks near 3674 cm^{-1}, which were caused by the symmetric and antisymmetric vibration containing -NH (typical wave number range is 3200 – 3500 cm^{-1}) in the

MBA, this shift was due to the reduction of hydrogen mass and the increase of vibration frequency after hydrogen bonds formation. As shown in Fig. 5, MBA had two identical and very active functional groups, which can be attached to CNF and PEG by hydrogen bonds and there were also hydrogen bonds between PEG and CNF. This double hydrogen bond structure ensured the strength and structural stability of CNPCMs. In addition, the spectra of CNPCMs were the same as that of PEG, indicating that only physical adsorption occurred between CNF and PEG, and no chemical reaction occurred.

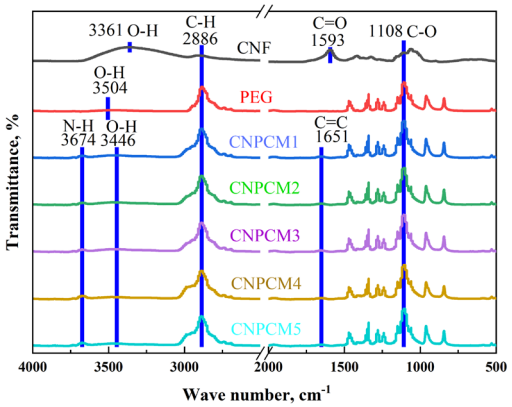

Fig. 4. FTIR spectra of CNF aerogel, PEG and CNPCMs

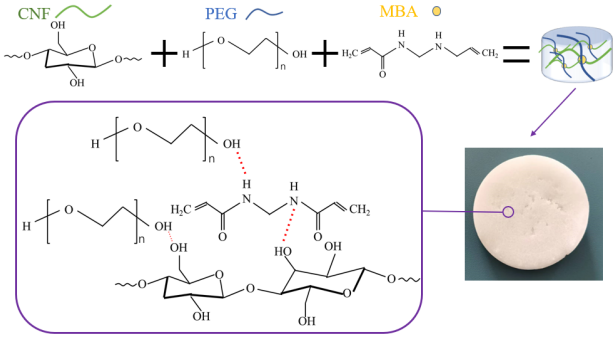

Fig. 5. Possible structural scheme of CNPCMs

3.4. XRD analysis

The X-ray diffraction (XRD) patterns of CNF aerogel, PEG, and CNPCMs were shown in Fig. 6. CNF was amorphous [34], so there was no intricate peak spectrum structure. In contrast, PEG had an excellent crystal structure, showing two sharp characteristic peaks at 19.2° (120 facet) and 23.3° (032 facet) [10]. The peak strength of CNPCM2 was higher than that of other samples which indicates that the crystal texture was formed at this ratio. Crystal texture was an important tool for the design and improvement of material properties, which had a significant impact on the physical, chemical, and mechanical properties of materials [35]. Therefore, CNPCMs still had the characteristic peak of PEG, but the change of its peak strength indicated that the crystal structure of PEG was affected, which in turn affected the phase change behavior and heat storage performance of CNPCMs.

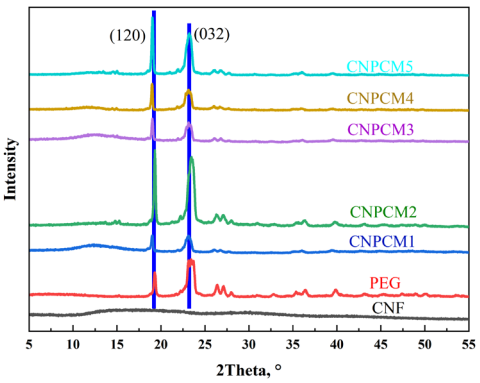

Fig. 6. XRD patterns of CNF aerogel, PEG and CNPCMs

3.5. Thermal properties analysis

The phase change properties of PEG and CNPCMs were analyzed by differential scanning calorimetry (DSC). The DSC curves of PEG and CNPCMs were tested at a heating/cooling rate of 10 ℃/min, as shown in Fig. 7 a and Fig. 7 b. Table. 1 shows the corresponding values of solidification temperature (T_s), solidification enthalpy (ΔH_s), melting temperature (T_m), and melting enthalpy (ΔH_m). The melting enthalpy of PEG was 181.2 J/g, and the solidification enthalpy of PEG was 147.7 J/g. The melting and solidification temperatures of CNPCMs were about 62.5 ℃ and 35.5 ℃ respectively, which were not different from those of PEG. At the same time, the melting enthalpy value was lower than that of PEG, indicating that the addition of CNF as a supporting skeleton did not affect the melting and solidification temperature, but affected the enthalpy value. Fig. 7 b showed the DSC curves of the cooling process, in which CNPCM1, CNPCM3, CNPCM4, and CNPCM5 showed two peaks, among which CNPCM1 was more obvious. We believed that this phenomenon was caused by the inappropriate amount of PEG loaded in CNF. In CNPCM1, less PEG was loaded on CNF, so the part loaded with PEG started solidifying first, and the part CNF without PEG started solidifying later. CNPCM4 and CNPCM5 were loaded with more PEG, the overloaded PEG was solidified first, and the rest was then solidified. Although CNPCM3 had two peaks, its connection was smoother than CNPCM4 and CNPCM5, and we considered CNPCM3 to be the maximum load (78 % of PEG mass fraction). CNPCM2 was the best ratio, which was also confirmed by the XRD curves.

Table. 1. Phase change properties of PEG and CNPCMs

Samples	T_m, ℃	ΔH_m, J/g	T_s, ℃	ΔH_s, J/g
PEG	63.6	181.2	34.7	147.7
CNPCM1	63.5	179.5	35.4	156.1
CNPCM2	62.6	167.9	36.0	146.1
CNPCM3	62.5	175.4	35.7	145.2
CNPCM4	63.2	167.9	37.8	144.3
CNPCM5	61.9	161.7	35.2	142.1

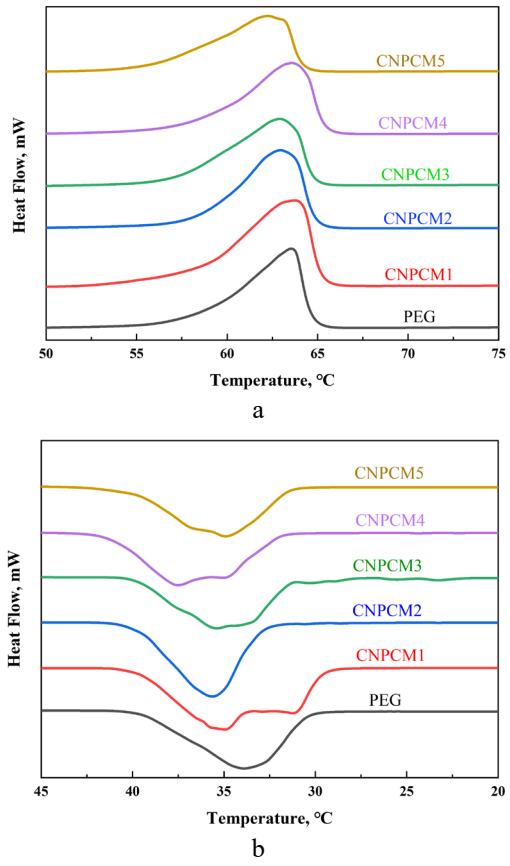

Fig. 7. a – melting DSC curves; b – solidifying DSC curves of PEG and CNPCMs

3.6. Thermal conductivity

The thermal conductivity of PCM was one of the important parameters for solar collector thermal energy storage applications because it significantly affected the rate of heat storage and release. The thermal conductivity of pure PEG and CNPCMs were analyzed by Hot Disk. The test conditions were carried out at an ambient temperature of 20 °C. The thermal conductivity of PEG and CNPCMs is shown in Fig. 8.

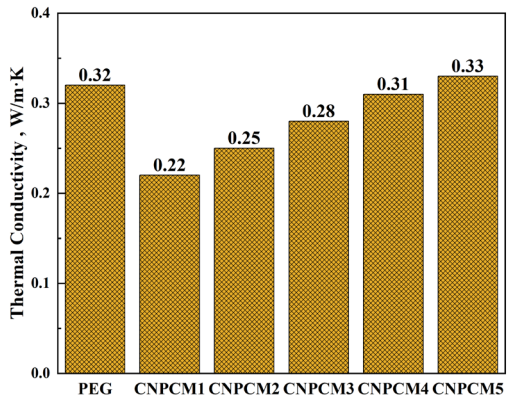

Fig. 8. The thermal conductivity of PEG and CNPCMs

The thermal conductivity of PEG was 0.32 W/m·K, and the thermal conductivity of CNPCMs increases with the increase of PEG mass fraction. The thermal conductivity of CNPCM1 was the lowest (0.22 W/m·K), the thermal conductivity of CNPCM2, CNPCM3 and CNPCM4 were 0.25, 0.28 and 0.31 W/m·K respectively, and thermal conductivity of CNPCM5 was 0.33 W/m·K, up to 103 % of the PEG. The experimental results showed that the addition of CNF separated PEG, prevented it from forming a continuous heat conduction channel, and led to a decrease in thermal conductivity. In the experimental and simulation studies in the field of solar collector heat storage, the thermal conductivity of PCMs used by some researchers was about 0.2 W/m·K, such as Hassan Olfian et al. [36].

Although the thermal conductivity of CNPCMs met the requirements, they can be considered to add high thermal conductivity packing to enhance the thermal conductivity and make it more widely used.

3.7. Thermal stability

The TGA results of CNF aerogel, PEG, and CNPCMs were shown in Fig. 9, demonstrating that CNPCMs had excellent durability in the operating temperature range below 100 °C and can be safely used for practical thermal energy storage. CNF aerogel underwent thermal decomposition at 50 °C with a T_{max} (temperature at the maximum rate of weight loss) of 302 °C.

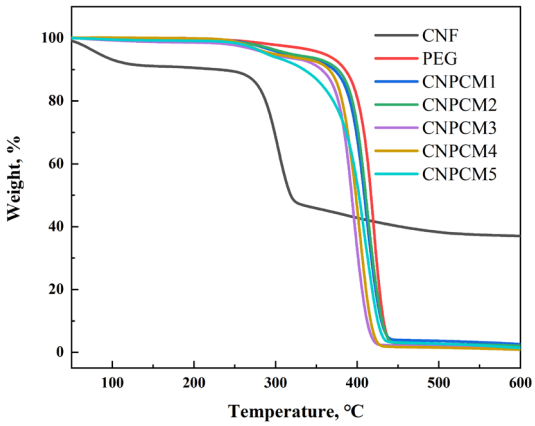

Fig. 9. TGA curves of CNF aerogel, PEG, and CNPCMs

The thermal decomposition behavior of PEG and CNPCMs was very similar, whose thermal decomposition process was in the range of 295 – 445 °C, and the T_{max} was about 410 °C. Compared with the relevant studies [23], the thermal stability of CNPCMs with double hydrogen bonds prepared by us was better.

3.8. Thermal exposure experiment analysis

The experimental samples with a mass of 0.8 g were sequentially placed (Fig. 10) on tinfoil and then placed in the oven to ensure continuous thermal exposure. Both PEG and CNPCMs did not show any signs of phase change when exposed to the oven at the temperature of 60 °C for 10 minutes; when exposed at 75 °C for 10 minutes, PEG and CNPCM5 just began to melt, and CNPCM4 melted into two parts, one part was melted overload PEG and the other part was gel; when exposed at 75 °C for 20 minutes, PEG, CNPCM4 and CNPCM5 melted completely, CNPCM3 also melted but remained gel, while CNPCM1 and CNPCM2 only showed initial signs of melting; when exposed at 75 °C for 25 minutes, CNPCM4 and CNPCM5 still tended to flow, while CNPCM3 gel did not change, and CNPCM1 and CNPCM2 also underwent solid-gel phase change without

leakage or any change in shape. The thermal exposure experiment showed that CNF was indeed an excellent supporting skeleton, and its excellent support and thickening properties provided strong support for the solid-gel phase change. It also confirmed that CNPCM2 was the best ratio in the experimental group. CNPCM3 was the maximum load ratio, beyond which solid-gel phase change could not be achieved.

Fig. 10. Digital photographs obtained by placing PEG and CNPCMs in the oven at 60 °C and 75 °C (PEG, CNPCM1, CNPCM2, CNPCM3, CNPCM4, and CNPCM5 from left to right)

4. CONCLUSIONS

This study innovatively used PEG as PCM, MBA as a physical crosslinking agent, and CNF as a supporting skeleton to obtain solid-gel phase change materials CNPCMs by simple melting polymerization, which provided ideas for the preparation of green and environmentally friendly composite phase change materials. Due to hydrogen bonding and the supporting effect of CNF, CNPCMs had good shape stability and thermal stability. The porous structure of CNF provided space for the volume change of PEG after the phase change, thus avoiding the leakage problem. The thermal exposure experiment and TGA experiment showed that CNPCMs had good durability and stability in the operating temperature range of 60 ~ 75 °C. The experimental results showed CNPCMs had excellent shape stability, thermal stability, and high enthalpy value, especially CNPCM2. The latent heat of melting and solidification of CNPCM2 were as high as 167.9 J/g and 146.1 J/g, respectively. Based on the outstanding performance of CNPCMs in heat storage capacity and structural stability, it can be applied in the field of waste heat recovery, aerospace equipment, and solar collector thermal management.

Acknowledgments

This work was financially supported by the Innovation Foundation for Postgraduate of Jiangxi (YC2022-s023).

REFERENCES

1. **Martins, F., Felgueiras, C., Smitková, M.** Fossil Fuel Energy Consumption in European Countries *Energy Procedia* 153 2018: pp. 107 – 111. https://doi.org/10.1016/j.egypro.2018.10.050
2. **Ji, J., Yu, X., Liu, Y.** Causality and Impulse Response on the Relationship Between Energy Consumption and Environmental Pollution: A Case Study of Qingdao City *In 2009 International Joint Conference on Computational Sciences and Optimization* 2 2009: pp. 485 – 488. https://doi.org/10.1109/CSO.2009.403
3. **Alva, G., Lin, Y., Fang, G.** An Overview of Thermal Energy Storage Systems *Energy* 144 2018: pp. 341 – 378. https://doi.org/10.1016/j.energy.2017.12.037
4. **Ding, Z., Wu, W., Leung, M.** Advanced/Hybrid Thermal Energy Storage Technology: Material, Cycle, System and Perspective *Renewable and Sustainable Energy Reviews* 145 2021: pp. 111088. https://doi.org/10.1016/j.rser.2021.111088
5. **Kerskes, H., Bertsch, F., Mette, B., Wörner, A., Schaube, F.** Thermochemical Energy Storage *Chemie Ingenieur Technik* 83 (11) 2011: pp. 2014 – 2026. https://doi.org/10.1002/cite.201100091
6. **Suresh, C., Saini, R.P.** Thermal Performance of Sensible and Latent Heat Thermal Energy Storage Systems *International Journal of Energy Research* 44 (6) 2020: pp. 4743 – 4758. https://doi.org/10.1002/er.5255
7. **Huang, L., Yang, Y., Yuan, D., Cai, X.** Solid-Solid Phase-Change Materials with Excellent Mechanical Property and Solid State Plasticity Based on Dynamic Urethane Bonds for Thermal Energy Storage *Journal of Energy Storage* 36 2021: pp. 102343. https://doi.org/10.1016/j.est.2021.102343
8. **Feng, L., Song, P., Yan, S., Wang, H., Wang, J.** The Shape-Stabilized Phase Change Materials Composed of Polyethylene Glycol and Graphitic Carbon Nitride Matrices *Thermochimica Acta* 612 2015: pp. 19 – 24. http://dx.doi.org/10.1016/j.tca.2015.05.001
9. **Li, M., Wang, C.** Preparation and Characterization of GO/PEG Photo-Thermal Conversion Form-Stable Composite Phase Change Materials *Renewable Energy* 141 2019: pp. 1005 – 1012. https://doi.org/10.1016/j.renene.2019.03.141
10. **Cheng, M., Hu, J., Xia, J., Liu, Q., Wei, T., Ling, Y., Li, W., Liu, B.** One-Step In-Situ Green Synthesis of Cellulose Nanocrystal Aerogel Based Shape Stable Phase Change Material *Chemical Engineering Journal* 431 2022: pp. 133935. https://doi.org/10.1016/j.cej.2021.133935
11. **Fallahi, A., Gulden tops, G., Tao, M., Granados-Focil, S., Van Dessel, S.** Review on Solid-Solid Phase Change Materials for Thermal Energy Storage: Molecular Structure and Thermal Properties *Applied Thermal Engineering* 127 2017: pp. 1427 – 1441. http://dx.doi.org/10.1016/j.applthermaleng.2017.08.161
12. **Zhou, Y., Sheng, D., Liu, X., Lin, C., Ji, F., Dong, L., Xu, S., Yang, Y.** Synthesis and Properties of Crosslinking Halloysite Nanotubes/Polyurethane-Based Solid-Solid Phase Change Materials *Solar Energy Materials and Solar Cells* 174 2018: pp. 84 – 93. http://dx.doi.org/10.1016/j.solmat.2017.08.031
13. **Fan, X., Guan, Y., Li, Y., Yu, H.Y., Marek, J., Wang, D., Militky, J., Zou, Z.Y., Yao, J.** Shape-Stabilized Cellulose Nanocrystal-Based Phase-Change Materials for Energy Storage *ACS Applied Nano Materials* 3 (2) 2020: pp. 1741 – 1748. https://dx.doi.org/10.1021/acsanm.9b02441
14. **Umair, M.M., Zhang, Y., Iqbal, K., Zhang, S.F., Tang, B.T.** Novel Strategies and Supporting Materials Applied to Shape-Stabilize Organic Phase Change Materials for Thermal Energy Storage – A Review *Applied Energy* 235 2019: pp. 846 – 873. https://doi.org/10.1016/j.apenergy.2018.11.017

15. **Gao, H., Wang, J., Chen, X., Wang, G., Huang, X., Li, A., Dong, W.** Nanoconfinement Effects on Thermal Properties of Nanoporous Shape-Stabilized Composite PCMs: A Review *Nano Energy* 53 2018: pp. 769 – 797. https://doi.org/10.1016/j.nanoen.2018.09.007
16. **Nechyporchuk, O., Belgacem, M.N., Bras, J.** Production of Cellulose Nanofibrils: A Review of Recent Advances *Industrial Crops and Products* 93 2016: pp. 2 – 25. http://dx.doi.org/10.1016/j.indcrop.2016.02.016
17. **Chen, J., Zhang, Y., Wu, F., Guan, B., Du, X., Wang, H.** Cellulose Nanofiber/Melanin Hybrid Aerogel Supported Phase Change Materials with Improved Photothermal Conversion Efficiency and Superior Energy Storage Density *Cellulose* 28 (15) 2021: pp. 9739 – 9750. https://doi.org/10.1007/ s10570-021-04152-7
18. **Colic, M., Tomic, S., Bekic, M.** Immunological Aspects of Nanocellulose *Immunology Letters* 222 2022: pp. 80 – 89. https://doi.org/10.1016/j.imlet.2020.04.004
19. **Zhang, F., Ren, H., Tong, G., Deng, Y.** Ultra-Lightweight Poly (Sodium Acrylate) Modified TEMPO-Oxidized Cellulose Nanofibril Aerogel Spheres and their Superabsorbent Properties *Cellulose* 23 (6) 2016: pp. 3665 – 3676. https://doi.org/10.1007/s10570-016-1041-8
20. **Mohan, D., Sajab, M.S., Kaco, H., Bakarudin, S.B., Noor, A.M.** 3D Printing of UV-Curable Polyurethane Incorporated with Surface-Grafted Nanocellulose *Nanomaterials* 9 (12) 2019: pp. 1726. https://doi.org/10.3390/nano9121726
21. **Chen, C., Li, C., Yu, D., Wu, M.** A Facile Method to Prepare Superhydrophobic Nanocellulose-Based Aerogel with High Thermal Insulation Performance via A Two-step Impregnation Process *Cellulose* 29 (1) 2022: pp. 245 – 257. https://doi.org/10.1007/ s10570-021-04275-x
22. **Wei, G., Zhang, J., Usuelli, M., Zhang, X., Liu, B., Mezzenga, R.** Biomass vs Inorganic and Plastic-based Aerogels: Structural Design, Functional Tailoring, Resource-Efficient Applications and Sustainability Analysis *Progress in Materials Science* 125 2022: pp. 100915. https://doi.org/10.1016/j.pmatsci.2021.100915
23. **Yazdani, M.R., Ajdary, R., Kankkunen, A., Rojas, O.J., Seppala, A.** Cellulose Nanofibrils Endow Phase-Change Polyethylene Glycol with Form Control and Solid-to-gel Transition for Thermal Energy Storage *ACS Applied Materials & Interfaces* 13 (5) 2021: pp. 6188 – 6200. https://dx.doi.org/10.1021/acsami.0c18623
24. **Gurav, J.L., Jung, I.K., Park, H.H., Kang, E.S., Nadargi, D.Y.** Silica Aerogel: Synthesis and Applications *Journal of Nanomaterials* 2010 2010: pp. 1 – 11. https://doi.org/10.1155/2010/409310
25. **Shen, J., Fu, S.** Research Progress of Cellulose-Based Hydrogels *Chemical Industry and Engineering Progress* 41 (6) 2022: pp. 3022 – 3037. https://doi.org/10.16085/j.issn.1000-6613.2021-1308
26. **Liang, L., Zhang, S., Goenaga, G.A., Meng, X., Zawodzinski, T.A., Ragauskas, A.J.** Chemically Cross-Linked Cellulose Nanocrystal Aerogels for Effective Removal of Cation Dye *Frontiers in Chemistry* 8 2020: pp. 570. https://doi.org/10.3389/fchem.2020.00570
27. **Long, L.Y., Weng, Y.X., Wang, Y.Z.** Cellulose Aerogels: Synthesis, Applications, and Prospects *Polymers* 10 (6) 2018: pp. 623. https://doi.org/10.3390/polym10060623
28. **Sun, Y., Chu, Y., Wu, W., Xiao, H.** Nanocellulose-Based Lightweight Porous Materials: A Review *Carbohydrate Polymers* 255 2021: pp. 117489. https://doi.org/10.1016/j.carbpol.2020.117489
29. **Wang, Z., Zhu, W.K., Huang, R.Z., Zhang, Y., Jia, C., Zhao, H., Chen, W., Xue, Y.Y.** Fabrication and Characterization of Cellulose Nanofiber Aerogels Prepared via Two Different Drying Techniques *Polymers* 12 (11) 2020: pp. 2583. https://doi.org/10.3390/polym12112583
30. **Zhang, M., Li, M., Xu, Q., Jiang, W., Hou, M., Guo, L., Wang, N., Zhao, Y., Liu, L.** Nanocellulose-Based Aerogels with Devisable Structure and Tunable Properties via Ice-Template Induced Self-Assembly *Industrial Crops and Products* 179 2022: pp. 114701. https://doi.org/10.1016/j.indcrop.2022.114701
31. **Yamagata, M., Uematsu, H., Maeda, Y., Suye, S., Fujita, S.** Bundling of Cellulose Nanofibers in PEO Matrix by Aqueous Electrospinning *Journal of Fiber Science and Technology* 77 (9) 2021: pp. 223 – 230. https://doi.org/10.2115/fiberst.2021-0024
32. **Tian, C., Liu, M., Lin, C., Lin, Y.** Preparation of Graft Copolymer of Cellulose and N, N'-methylenebisacrylamide Using Ionic Liquid as Reaction Medium *Journal of Cellulose Science and Technology* 19 (3) 2011: pp. 16 – 21. https://doi.org/10.3969/j.issn.1004-8405.2011.03.003
33. **Hai, L.V., Zhai, L., Kim, H.C., Panicker, P.S., Pham, D.H., Kim, J.** Chitosan Nanofiber and Cellulose Nanofiber Blended Composite Applicable for Active Food Packaging. *Nanomaterials* 10 (9) 2020: pp. 1752. https://doi.org/10.3390/nano10091752
34. **Ghalehno, M.D., Yousefi, H.** Toward Wheat Straw Valorization by Its Downsizing to Five Types of Cellulose Nanomaterials and Nanopapers Thereof *Waste and Biomass Valorization* 14 (9) 2023: pp. 2885 – 2896. https://doi.org/10.1007/s12649-023-02031-9
35. **Bunaciu, A.A., Udristioiu, E.G., Aboul-Enein, H.Y.** X-ray Diffraction: Instrumentation and Applications *Critical Reviews in Analytical Chemistry* 45 (4) 2015: pp. 289 – 299. https://doi.org/10.1080/10408347.2014.949616
36. **Olfian, H., Mousavi Ajarostaghi, S.S., Ebrahimnataj, M., Farhadi, M., Arıcı, M.** On the Thermal Performance of Evacuated Tube Solar Collector Integrated with Phase Change Material *Sustainable Energy Technologies and Assessments* 53 2022: pp. 102437. https://doi.org/10.1016/j.seta.2022.102437